Bioresource Technology 252 (2018) 91–99

Contents lists available at ScienceDirect

Bioresource Technology

journal homepage: www.elsevier.com/locate/biortech

Selective separation of microalgae cells using inertial microfluidics

Maira S. Syed[a,b,*,1], Mehdi Rafeie[a,1], Dries Vandamme[b,d], Mohsen Asadnia[c], Rita Henderson[b], Robert A. Taylor[a,e], Majid E. Warkiani[f,g,*]

[a] School of Mechanical and Manufacturing Engineering, University of New South Wales, Australia
[b] Biomass Lab, School of Chemical Engineering, University of New South Wales, Australia
[c] Department of Engineering, Macquarie University, Sydney, New South Wales, Australia
[d] Laboratory for Aquatic Biology, KU Leuven, Campus Kulak, Belgium
[e] School of Photovoltaic and Renewable Energy Engineering, University of New South Wales, Australia
[f] School of Biomedical Engineering, University of Technology Sydney, Australia
[g] Center for Health Technologies, University of Technology Sydney, Australia

ARTICLE INFO

Keywords:
Tetraselmis suecica
Phaeodactylum tricornutum
Selective separation
Spiral microchannel

ABSTRACT

Microalgae represent the most promising new source of biomass for the world's growing demands. However, the biomass productivity and quality is significantly decreased by the presence of bacteria or other invading microalgae species in the cultures. We therefore report a low-cost spiral-microchannel that can effectively separate and purify *Tetraselmis suecica* (lipid-rich microalgae) cultures from *Phaeodactylum tricornutum* (invasive diatom). Fluorescent polystyrene-microbeads of 6 μm and 10 μm diameters were first used as surrogate particles to optimize the microchannel design by mimicking the microalgae cell behaviour. Using the optimum flowrate, up to 95% of the *P. tricornutum* cells were separated from the culture without affecting the cell viability. This study shows, for the first time, the potential of inertial microfluidics to sort microalgae species with minimal size difference. Additionally, this approach can also be applied as a pre-sorting technique for water quality analysis.

1. Introduction

Microalgae are unicellular organisms that form the base of the marine food chain in oceans. Microalgae have garnered major global interest in recent years as a promising source of cultivated biomass (Ruiz et al., 2016). This is due to their potential for high-efficiency biofuel production (Huang and Su, 2014), their higher biomass productivity than terrestrial plants (Wan et al., 2015), their capacity to grow on non-arable land using marine/waste water (Rodolfi et al., 2009), their carbon dioxide capture potential (Chisti, 2007), and their use as feedstocks for production of high value products (Brennan and Owende, 2010). Unfortunately, microalgal cultures are often vulnerable to contamination from invading bacteria or other microalgae species (Bartley et al., 2013; Goldman et al., 1982). For physiological studies as well as for biomass production, stable cultures are desired. Contaminating microorganisms cause nutrient competition which results in an overall decrease of biomass productivity, composition and quality (Sensen et al., 1993). *Phaeodactylum tricornutum* is a marine diatom that can survive in very harsh conditions and has the capability to outcompete the other species such as *Dunaliella* sp. *or Tetraselmis* sp. in a co-culture, especially at extreme pH (Goldman et al., 1982; Goldman and Stanley, 1974). This indicates a clear need to control, mediate, or prevent its incursion to minimize the risk of partial or complete takeover of large-scale cultures (Goldman and Stanley, 1974).

Traditional methods to mitigate contaminated laboratory cultures include laborious microscopy and micropipetting (Hoshaw and Rosowski, 1973), culturing on a selective medium in agar plates (Koch, 2010), or using serial dilution techniques (Sinigalliano et al., 2009). In the lab, flow cytometry (FCM) equipped with a cell-sorting module can also be used for efficient differentiation and subsequent isolation of single cells based upon their morphology (size) and variations in fluorescence (Cellamare et al., 2010; Sensen et al., 1993). FCM sorting techniques, however, have very high operation and maintenance cost, and frequently cause cell damage (due to exposure to optical, electrical, and mechanical perturbations) (Cellamare et al., 2010). Microflow cytometer prototypes have been developed to reduce the cost while achieving the same resolution of separation as conventional FCM (Hashemi et al., 2011). However, since these systems use relatively powerful laser sources and high-resolution sensors, their implementation has been limited to lab-based studies. To the author's knowledge,

* Corresponding authors at: School of Mechanical and Manufacturing Engineering, University of New South Wales, Australia (M.S. Syed). School of Biomedical Engineering, University of Technology Sydney, NSW 2007, Australia (M.E. Warkiani).
E-mail addresses: maira.syed@student.unsw.edu.au (M.S. Syed), majid.warkiani@uts.edu.au (M.E. Warkiani).
[1] These authors contributed equally.

https://doi.org/10.1016/j.biortech.2017.12.065
Received 23 October 2017; Received in revised form 19 December 2017; Accepted 20 December 2017
Available online 21 December 2017
0960-8524/

no technology has been developed to date which can achieve effective, yet low-cost, separation, fractionation, and enrichment of microalgal cultures.

Recently microfluidic-based techniques have gained prominence as efficient and powerful tools for high throughput control and focusing of micro-particles or cells based on size and morphology (Di Carlo, 2009; Rafeie et al., 2016). These microfluidic separation techniques can be broadly classified as 'active' or 'passive'. Passive technologies are often favored since they offer low cost and effective separation without external forces (aside from pumping power). Active techniques use energy consuming magnetic (Iliescu et al., 2008) or acoustic (Augustsson et al., 2012) fields for operation, whereas passive techniques simply rely on the channel's geometry and intrinsic hydrodynamic forces (Rafeie et al., 2016). Writ large, these emerging microfluidic technologies have made dramatic advances in a wide range of biomedical (Rafeie et al., 2016; Wu et al., 2012), point of care (Yetisen et al., 2013), drug screening (Skommer and Wlodkowic, 2015), environmental analysis (Jokerst et al., 2012), chemical and biological detection (Sei et al., 2014), and other applications. On the subject of this report, these microfluidic systems have been employed for on-chip detection of microalgal cells (Li et al., 2016), cell culturing (Paik et al., 2017), cell sorting (Juang and Chang, 2016; Schaap et al., 2016), gene sequencing and genome studies (Ghim et al., 2010), cell lysis (Wu et al., 2011), harvesting (Hønsvall et al., 2016; Shakeel Syed et al., 2017) and microbial bioenergy (Han et al., 2013) applications. So far, though, no studies have applied microfluidic-based technologies to the challenge of mitigating microalgae culture contamination.

The aim of this study is to demonstrate the potential of a low-cost, spiral inertial microfluidic device for selective separation of microalgae species on the basis of their different sizes and shapes, in order to achieve stable cultures of the desired strains. A mixed culture of *Tetraselmis suecica* and a common invading diatom, *Phaeodactylum tricornutum*, was used as a model system to be purified. Fluorescent polystyrene microbeads were first used to optimize the microchannel design by mimicking the behaviour of both of these microalgal cell types. Secondly, selective separation of the *P. tricornutum* from the *T. suecica* cells was achieved by optimizing flow rates, cell concentration and cultivation time. Finally, cell viability was analysed after separation.

2. Materials and methods

2.1. Theoretical analysis

Randomly dispersed particles/cells entering a straight microchannel are known to disturb the flow pattern and cross streamlines to eventually focus in certain lateral positions of the channel (Segre, 1961). This phenomenon, which is called inertial focusing, happens under the influence of three major lift forces.

The first component, called the shear gradient lift force (F_{LS}), arises from the difference of the velocity magnitude in adjacent fluid elements, creating a shear rate at each point. The interaction of the particles and this shear flow (i.e., F_{LS}) propels particles towards areas with higher shear rates. As a result, particles near the channel center are pushed towards channel walls. If particles approach the near-wall region, though, they disturb the flow pattern in a way that the pressure between them and the channel wall increases.

The second component, called the wall-induced lift force (F_{LW}), is caused by the pressure gradient near the wall which counteracts F_{LS} and propels the particles back towards the channel center. As can be seen in Fig. 1A-i, buoyant cells which were previously dispersed in a straight microchannel, gather in positions where these components of the inertial lift force are in balance.

The third component is a smaller force called the rotation induced lift force ($F_{L\Omega}$) (Guan et al., 2013; Zhou and Papautsky, 2013). This force arises from the rotation of the particles and it depends on the sign of shear rate and on the sign of the slip velocity of the particle. Zhou and Papautsky (2013) explained that once an initial equilibrium is reached in a straight microchannel, $F_{L\Omega}$ becomes dominant and gradually drags particles to the center point of all four of the channel walls (Fig. 1A-ii).

When particle size is small with respect to the channel's hydraulic diameter (Asmolov, 1999; Di Carlo, 2009), the net inertial lift force is expressed as follows.

$$F_L = \frac{\rho U^2 a^4}{D_h^2} f_L(Re, Z_C) \tag{1}$$

where ρ is fluid density, U is maximum velocity, a is the particle diameter, and D_h is the hydraulic diameter of the channel. The term $f_L(Re, z_C)$ is the lift coefficient of the net inertial lift force, which is a function of the normalized position of particles within the cross-section of the channel (z_C), and Re denotes the Reynolds number, defined as

$$Re = \frac{\rho U D_h}{\mu} \tag{2}$$

where μ is dynamic viscosity of the fluid (Di Carlo, 2009). The lift coefficient f_L is an unknown function which can be obtained through numerical simulations (Di Carlo et al., 2009), asymptotic analyses (Hood et al., 2015), or experimental measurements (Zhou and Papautsky, 2013).

The introduction of curvature to a straight microchannel induces an important secondary flow that directs the fluid from the inner side to the outer side of the curved channel. However, this secondary flow also returns through the regions near the channel's top and bottom walls. Therefore, in a curved microchannel, two counter rotating vortices develop, which are known as Dean vortices (Di Carlo, 2009). The velocity of this secondary flow (U_D) can be approximated as: (Bhagat et al., 2010; Kemna et al., 2012)

$$U_D = 1.8 \times 10^{-4} De^{1.63} \tag{3}$$

where De is the Dean number, $De = Re\,(D_h/2R)$, and R represents the radius of curvature for a spiral microchannel (Berger et al., 1983). Dean flow, in turn, creates an additional force called the Dean drag force (F_D) that can be used to manipulate the focusing behaviour of particles in the microchannel. Assuming the Stokes' drag law holds, F_D can be evaluated as: (Kuntaegowdanahalli et al., 2009)

$$F_D = 3\pi\mu a U_D \tag{4}$$

Thus, four forces must now be considered to find the final position of the focusing band(s) in spiral microchannels (Di Carlo et al., 2007). The magnitude of F_D can be equal to, larger, or smaller than F_L depending on the flow rate and geometry (Note that F_L is the resultant of the three components of inertial lift force). At very low flow rates, the magnitude of these forces is too small to cause the particles to focus. In this case particles remain (uselessly) dispersed in the channel. Alternatively, at very high flow rates F_D becomes dominant and forces particles to follow the secondary flow, which again disperses rather than focusing the particles. Therefore, a 'goldilocks' flow rate range exists which brings about the formation of only one sharp equilibrium positon. In a trapezoidal spiral microchannel, different potential focusing positions exist near both of the inner and outer side walls where F_L as well as F_D are in balance. For a certain particle size, the Dean flow aids particle focusing in one of these potential positions only. For larger particles, near the channel's top and bottom walls, reversed F_D is accompanied by the horizontal component of F_{LS} to drive particles towards the inner wall (i.e., locations ① and ② in Fig. 1A-iii). If larger particles (e.g., *T. suecica*) reach the near wall region, they do not follow Dean vortices anymore because F_{LS} counteracts them near the center of the channel, creating a force balance where larger particles can effectively focus at location ③ in Fig. 1A-iii). For smaller particles, however, F_{LS} is weaker and cannot compete with F_D in this location. As a result, smaller particles (e.g., *P. tricornutum*) follow the secondary flow until

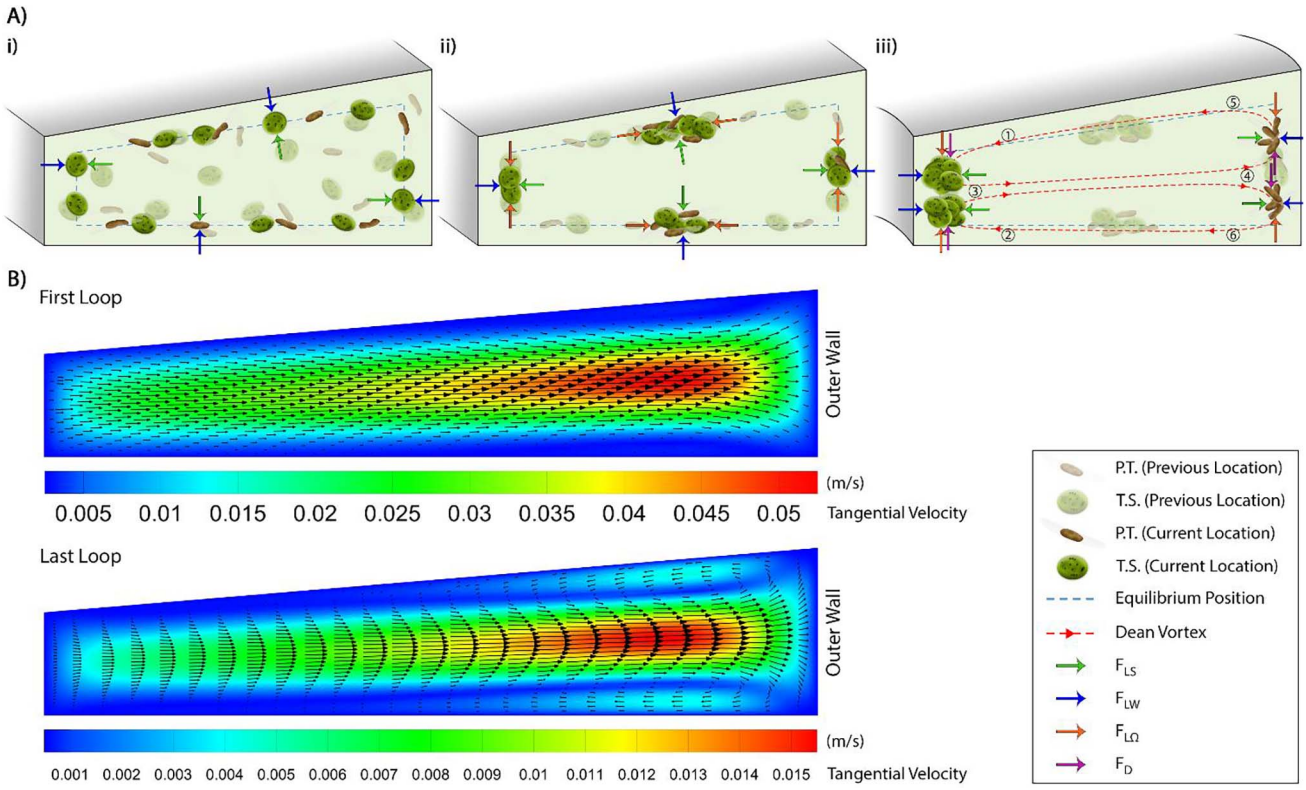

Fig. 1. (A) Cross-sectional view of microalgae undergoing inertial focusing. (i) In a straight microchannel with a slanted cross-section, cells focus on equilibrium lines where F_{LS} equals F_{LW}. (ii) After travelling a longer distance, particles/cells focus on the same equilibrium lines, but also in the middle of the channel walls due to the influence of $F_{L\Omega}$. (iii) In a curved channel of the same cross-section, centrifugal forces act on the fluid and induce Dean flow. These secondary flow relocates the equilibrium positions of (i) and (ii) since F_{LS}, F_{LW}, $F_{L\Omega}$, must now also balance with a Dean drag force, F_D. (B) Tangential velocity contours obtained from numerical simulation (using ANSYS-FLUENT®) in the first and last loops of a spiral channel for the microchannel geometry used in this work. In the last loop, the secondary flow vortices in the center of the channel push particles/cells towards the outer wall. (P.T.: *P. tricornutum*, T.S.: *T. suecica*).

they reach near outer wall region (i.e., location ④ in Fig. 1A-iii). In this region, reversed Dean vortices are weak and cannot entrain smaller particles again, creating separate focusing positions (e.g., locations ⑤ and ⑥ in Fig. 1A-iii) where small particles can focus. This difference in focusing behaviour of large and small particles, which is mainly a function of flow rate, provides an opportunity for the fractionation of particles/cells with different sizes. Supplementary Info provides a quantitative analysis of the particle focusing in this trapezoidal microchannel.

2.2. Microfluidic channel: design and fabrication

The spiral microchannel used in this work has eight circular loops, one inlet, and two outlets located at the center of the microchip. The cross-section of the slanted microchannel is trapezoidal with a width of 600 µm, and an inner and outer height of 80 µm and 130 µm, respectively (as shown in Fig. 2C). This particular design of spiral microchannel was chosen due to its capability to separate particles/cells with a small difference in size (Guan et al., 2013; Wu et al., 2012).

The spiral channels were made of polydimethylsiloxane (PDMS, Sylgard 184 Silicone Elastomer Kit, Dow Corning) using soft lithography from an aluminum mold manufactured using a micro-mill (Whits Technologies, Singapore). Degassed PDMS, mixed in a 10:1 ratio of the base: curing agent, was poured onto the aluminum mold. The PDMS was peeled off after baking for 2 h inside an oven at 65 °C. At this point, fluidic access holes were punched using a Uni-Core™ Puncher (Sigma-Aldrich Co. LLC. SG). Finally, the PDMS was irreversibly bonded with a thick PDMS slab using an oxygen plasma cleaner (PDC-002, Harrick Plasma, Ossining, NY).

2.3. Microalgae cultivation and sample preparation

A mixed culture of *T. suecica* and the marine diatom *P. tricornutum* was used as model system to be purified. Axenic cultures of both of these species (*P. tricornutum* and *T. suecica* CS-56/7) were obtained from Australian National Algae Culture Collection (ANACC), Hobart Australia. *P. tricornutum* are fusiform, with average major and minor diameters of approximately 25.7 ± 3.5 µm and 3.5 ± 0.2 µm, respectively. *T. suecica* cells are motile and prolate spheroid in shape, with an average maximum linear dimension of roughly 10.7 ± 0.8 µm (Lama et al., 2016). Both of the species were cultured separately and as a mixture in an autoclaved F/2 marine medium in 250 mL shake flasks. The cultures were grown in a temperature cycling chamber incubator (Labec, Australia), and were subject to a 16/8 h light/dark cycle with associated temperature control at 23 °C. The cultures were shaken daily by hand to ensure nutrients homogeneity and agglomerates dispersion. Upon the onset of the stationary growth phase (8–10 days), as determined by cell counting using a Bright-Line™ hemacytometer and an optical microscope (Leica DM750 Microscope, Germany), the cells were input to the microchannel for separation and purification tests.

2.4. Experimental setup and procedure

Experiments were first performed with fluorescent polystyrene microbeads (Fluoresbrite® Microspheres, Polysciences Inc, Singapore), which served as surrogate particles (of well-known diameter) for *P. tricornutum* and *T. suecica* cells. The sizes of the microbeads were selected based on the mean effective spherical diameters (ESD) calculated from the cell volume (Lama et al., 2016; Li et al., 2012). Therefore, particles sizes of 6 µm and 10 µm could mimic the behaviour of *P.*

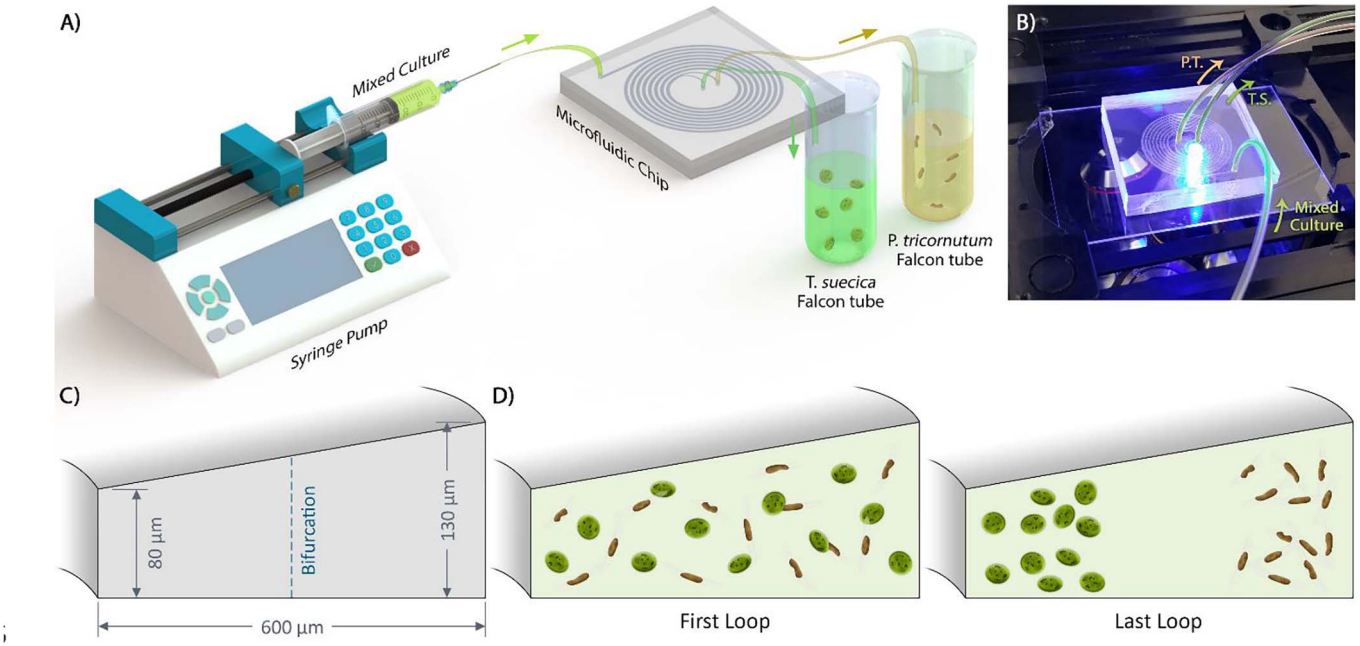

Fig. 2. (A) Schematic illustration of the experimental set-up for microalgae cells separation using a spiral channel with a trapezoidal cross-section. (B) Picture of the microfluidic device mounted on the fluorescent microscope. (C) The geometry of the channel's cross-section with a bifurcation in the middle of the channel. (D) Cartoon of the first loop mixture of *P. tricornutum* and *T. suecica* cells, compared to the separation that occurs by the last loop under the influence of F_L and F_D.

tricornutum and *T. suecica*, respectively. Thus, two particle suspensions of 1 µL/mL (i.e. 2.1×10^5 particles/mL for 6 µm and 0.45×10^5 particles/mL for 10 µm beads) were prepared in a buffer solution having 1× phosphate buffered saline (PBS) and 2 mM EDTA, augmented with 0.5% bovine serum albumin (BSA) (MiltenyiBiotec, Germany). BSA was added to avoid adhesion of the microbeads to channel walls and tubing.

For in-situ characterization of the fluorescent microbeads, the spiral microchip was placed on an inverted epifluorescence microscope with a CCD camera (Olympus IX73 microscope and Olympus DP80 camera, Olympus Inc., USA). The particle suspensions were injected into the microchannel using a syringe pump (Chemyx Fusion 200, Chemyx Inc., USA). This enabled both particle sizes to be directly observed at various steady flow rates ranging from 0.5 to 2 mL/min. Thus, the fluorescent signal intensity was observed at the point of bifurcation of the channel (Fig. 2).

For visualization of live *P. tricornutum* and *T. suecica* cells inside the spiral microchannel, the trajectories of the pure cultures were captured using an inverted fluorescence microscope (Nikon Eclipse TE 2000-S, Nikon instruments Inc., USA) equipped with a high-speed camera (FASTCAM SA5, Photron Inc., USA). Before loading the microalgae samples, the system was flushed with 70% ethanol and distilled water for deaerating and sterilizing the microchannels and tubing. A similar flow rate optimization was repeated for the *P. tricornutum* and *T. suecica* cultures. For this purpose, the trajectories of pure cultures of both species were captured and recorded by the high-speed camera at 8000 frames/s for all the flow rates at the same point of bifurcation. To depict cell trajectories, the difference between each frame of the video file and a reference frame were obtained using Adobe After Effects® software. The reference frame displays the microchannel without any cells. As a result, each of the new frames highlights the location of cells in the channel because everywhere else has no difference with the reference frame. Finally, we used the 'CC Time Blend' effect of the software to save and compare all of these differences over consecutive frames.

For quantification of the degree of cell sorting, samples from both the outlets were collected and cell concentrations of the samples were determined before and after the separation, via cell counting using the hemacytometer. The performance of the inertial microfluidic device for culture purification and cell sorting can be most appropriately expressed in terms of *P. tricornutum* focusing, *T. suecica* focusing, and fractionation efficiency. *P. tricornutum* focusing is the percentage of *P. tricornutum* cells exiting through the outer outlet. It should be noted that this percentage is same as the overall purification efficiency. Similarly, *T. suecica* focusing is the percentage of *T. suecica* cells collected at the inner outlet. Lastly, fractionation efficiency can be calculated as the difference in the percentages of *P. tricornutum* and *T. suecica* cells captured at the inner outlet.

The flow rate optimization was repeated with mixed culture samples, for the same range of flow rates. During the cell experiments, the effect of concentration of invading cells was tested by increasing the concentration of *P. tricornutum* cells from 3 to 60×10^5 cells/mL while keeping the concentration of *T. suecica* cells at $\sim 3 \times 10^5$ cells/mL. Finally, the purification experiments were repeated as a function of cultivation time at the optimum flow rate. Cell concentration and cell circularity of *T. suecica* were also analysed as a function of cultivation time in the feed and in the inner outlet using image analysis. To accomplish this, the cells were photographed using an optical microscope equipped with a digital camera (two duplicate pictures per sample, each containing 30–500 cells). The images were transformed to an 8-bit image where the background was subtracted. Cells were counted only when they were above a threshold minimum of 100 pixels, using image analysis software (Image J, NIH USA). The circularity and the effective spherical diameter (ESD) were determined based on the pixel area and perimeter and were calculated as follows (Heyt and Diaz, 1975):

$$Circularity = 4\pi \frac{Area}{Perimeter^2} \quad (5)$$

$$ESD = \frac{1.55 Area^{0.25}}{Perimeter^{0.25}} \quad (6)$$

2.5. Cell viability

The viability of cells before and after flow through the spiral microchannel was analysed using a Propidium Iodide (PI) staining essay – a commonly used method in microalgae and diatom cell viability essays

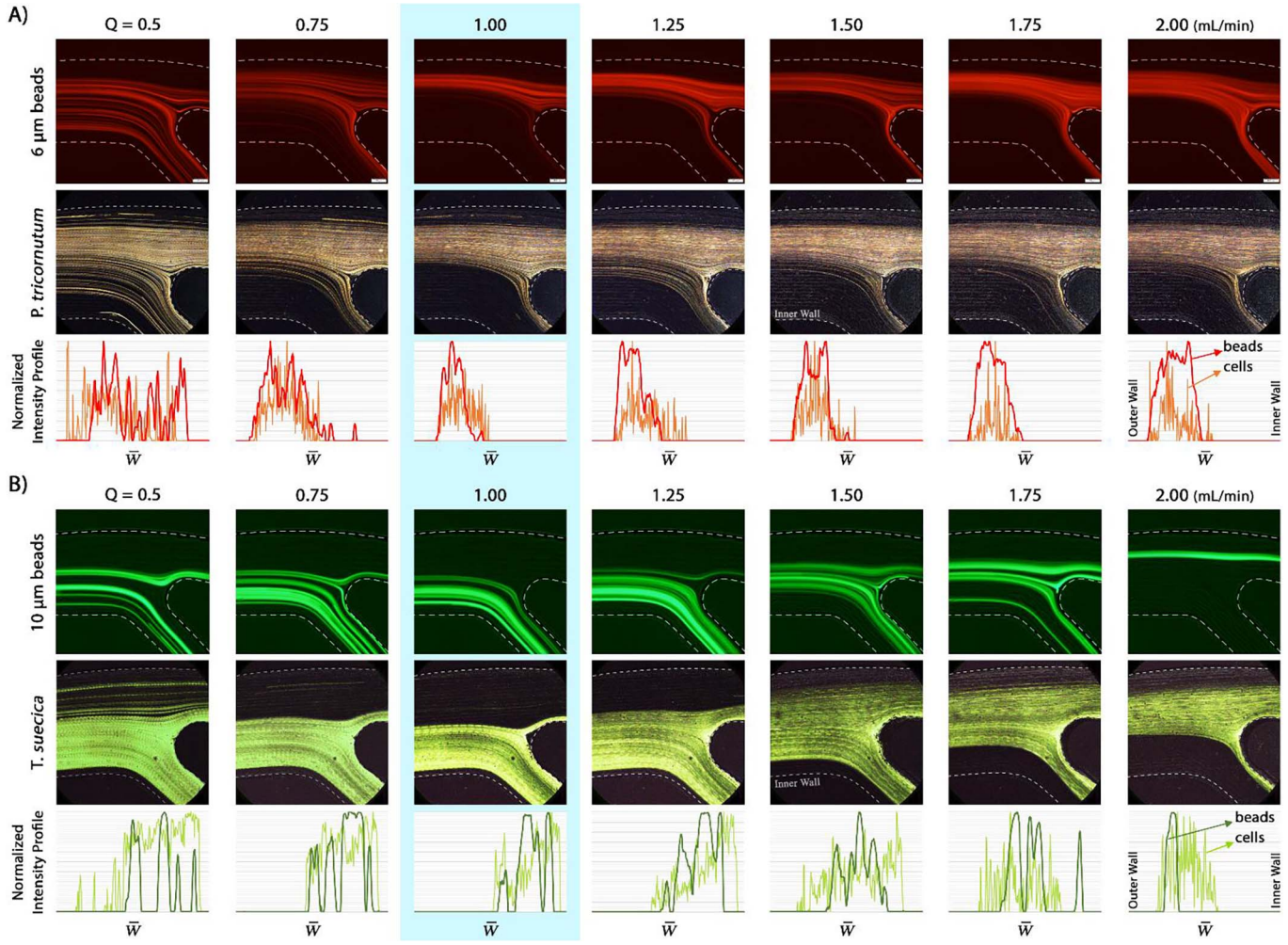

Fig. 3. (A) First row: Trajectories of the 6 µm fluorescent microbeads at the outlet of the trapezoidal section spiral microchannel at flow rates ranging from 0.5 to 2 mL/min. Second row: P. *tricornutum* cell trajectories under the same conditions Third row: Normalized intensity profiles of both the beads and cells at each flow rate. $\overline{W}$ denotes normalized width of the channel. (B) Similar to (A), the first row shows trajectories of the 10 µm fluorescent microbeads while the second row shows *T. suecica* cell trajectories, and the third row compares the intensity profiles of the beads with cells. Note that the best flow rate for the fractionation of particles/cells is Q = 1 mL/min.

(Hyka et al., 2013). As a reference for damaged cells, analogous samples were heated at 65 °C for 10 min. A 50 mg/L working solution of PI was prepared in milli-Q water and kept at 4 °C and protected from light. Then, 133 µL of this PI working solution was then added to 1 mL of the sample to be stained, to get a final concentration of 6.68 mg/L or 10 µM. After mixing, the sample was incubated for at least 15 min at room temperature in dark. The incubated samples were analysed using the flow cytometer (BD Accuri C6, Becton, Dickinson and Company, US).

3. Results and discussion

3.1. Separation of fluorescent microbeads

The monodisperse fluorescent polystyrene microbeads were tested first (top row of Fig. 3A and B). At low flow rates (i.e., Q ≤ 0.5 mL/min), the 6 µm microbeads remain dispersed in the channel. At Q = 0.75 mL/min, these microbeads start to roughly focus in the outer half of the channel. By increasing the flow rate, almost all of these particles go through the outer outlet at Q = 1 mL/min with approximately 92% focusing efficiency. At higher flow rates, however, the width of the focusing band increases slightly and many particles exit through both outlets. A similar trend can be seen for the 10 µm microbeads. The 10 µm microbeads focus roughly within the inner outlet of the channel at Q ≤ 0.75 mL/min and the focusing band becomes narrower at 1 mL/min, such that almost all of the particles are directed to the inner outlet. By increasing the flow rate, due to the influence of F_D, the focusing band of these particles travels towards the outer half of the channel and progressively approaches the outer wall until all of them focus sharply near the outer wall of the channel at Q = 2 mL/min. A comparison between the results of both particle sizes suggests that the selective cells sorting based on size could be achieved at 1 mL/min using this well-chosen spiral microchannel design.

3.2. Selective separation of microalgae

Based on the optimum flow rates obtained using the fluorescent microbeads, similar tests were conducted with microalgae cells. The behaviour of both *P. tricornutum* and *T. suecica* cells were visually observed using the high-speed camera and the separation performance was quantified based on cells counts.

3.2.1. Visualization of cell trajectories

The cell trajectories acquired from the processed videos of pure cultures of *P. tricornutum* and *T. suecica* was in fair agreement with the traces of the corresponding fluorescent microbeads (Fig. 3A and B). However, the focusing bands of the cells were wider than for the microbeads. It is presumed that the cell heterogeneity and the non-

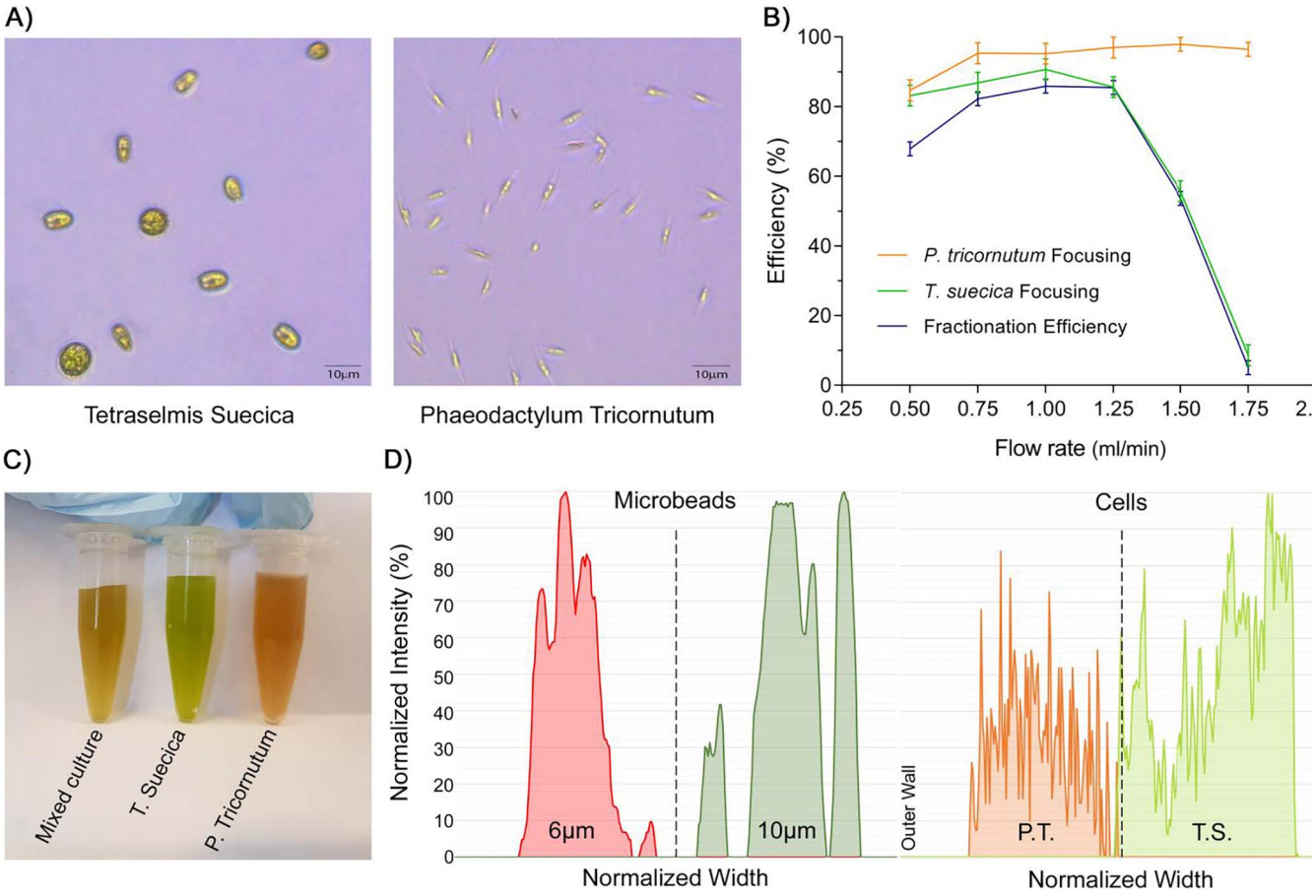

Fig. 4. A) Micrographs for *T. suecica* and *P. tricornutum* cells. B) Results for flow rate optimization based on cell counts. The optimal fractionation was found to occur at 1 mL/min. C) Photographs of mixed culture and separated cultures. (I) Mixed culture, (II) separated *T. suecica* cells, and (III) separated *P. tricornutum* cells. D) Comparison of the intensity profiles for the cells and microbeads at 1 mL/min. The dash lines represent the bifurcation position.

sphericity of the microalgae cells is the underlying cause of the wider focusing band compared to the standard, spherical polystyrene microbeads. However, these results also indicate that Q = 1 mL/min was the optimal flow rate to maximize separation of these cells; which is in agreement with the tests using the standard microbeads

3.2.2. Flow rate optimization based on cell counts

Fig. 4 shows the results for the quantitative analysis of the performance of the spiral microchannel for sorting microalgae cells, based on cells counts. For Q = 0.5 mL/min, 80% of the *P. tricornutum* cells were collected through the outer outlet. For all the flow rates between Q = 1 mL/min and 1.75 mL/min, *P. tricornutum* focusing efficiency was more than 90% (Fig. 4B). The behaviour of the *T. suecica* cells varied substantially with flow rate. The *T. suecica* focusing efficiency increased from 83% to 91% as the flow rate increased from Q = 0.5 mL/min to 1 mL/min. A further increase in the flow rate caused a significant decline in *T. suecica* focusing, until only 8% of cells were captured in the inner outlet at Q = 1.75 mL/min. Finally, the fractionation efficiency was the highest at Q = 1 mL/min, which additionally confirms that the respective microbeads can be used as a reference for mimicking the behaviour of these microalgae cells. In addition to separation of the cells, there was also an increase in the concentration of each species exiting through the respective outlets. At 1 mL/min, the concentration of both *P. tricornutum* and *T. suecica* was roughly twice of their initial concentration (data not shown).

3.3. Feasibility and implementation of inertial microfluidic technology for algae separation

Now that it has been verified that *P. tricornutum* and *T. suecica* cells can be fractionated, there are several other factors that need to be investigated to determine practicality and implementation of this technique, so the following were also investigated: cell viability, effect of *P. tricornutum* concentration, and effect of contamination ratio, and purification efficiency over time.

3.3.1. Cell viability analysis

There is a risk for cell damage by the forces experienced inside the channel which could make this technology unsuitable for this application. Thus, the cell viability in the inner and outer outlet at the flow rate of 1 mL/min was compared to the feed and a reference sample of damaged cells both for *P. tricornutum* and *T. suecica* cells (Fig. 5A). The reference sample for damaged cells showed a large peak shift to the right, which indicates that the fluorescent stain entered the cell walls. However, there was no similar peak shift observed for either outlet sample compared to the feed, so it can be concluded that there is no measurable change in viability of the cells that went through the microchannel device.

3.3.2. Effect of P. tricornutum concentration on purification efficiency

The purification efficiency at Q = 1 mL/min was determined at various *P. tricornutum* cell concentrations (Fig. 5B). In these tests, only a minor decrease in efficiency was observed as the *P. tricornutum* concentration increased from 0.3 million cells/mL to 6 million cells/mL. Regardless of the degree of contamination, the efficiency of removal of

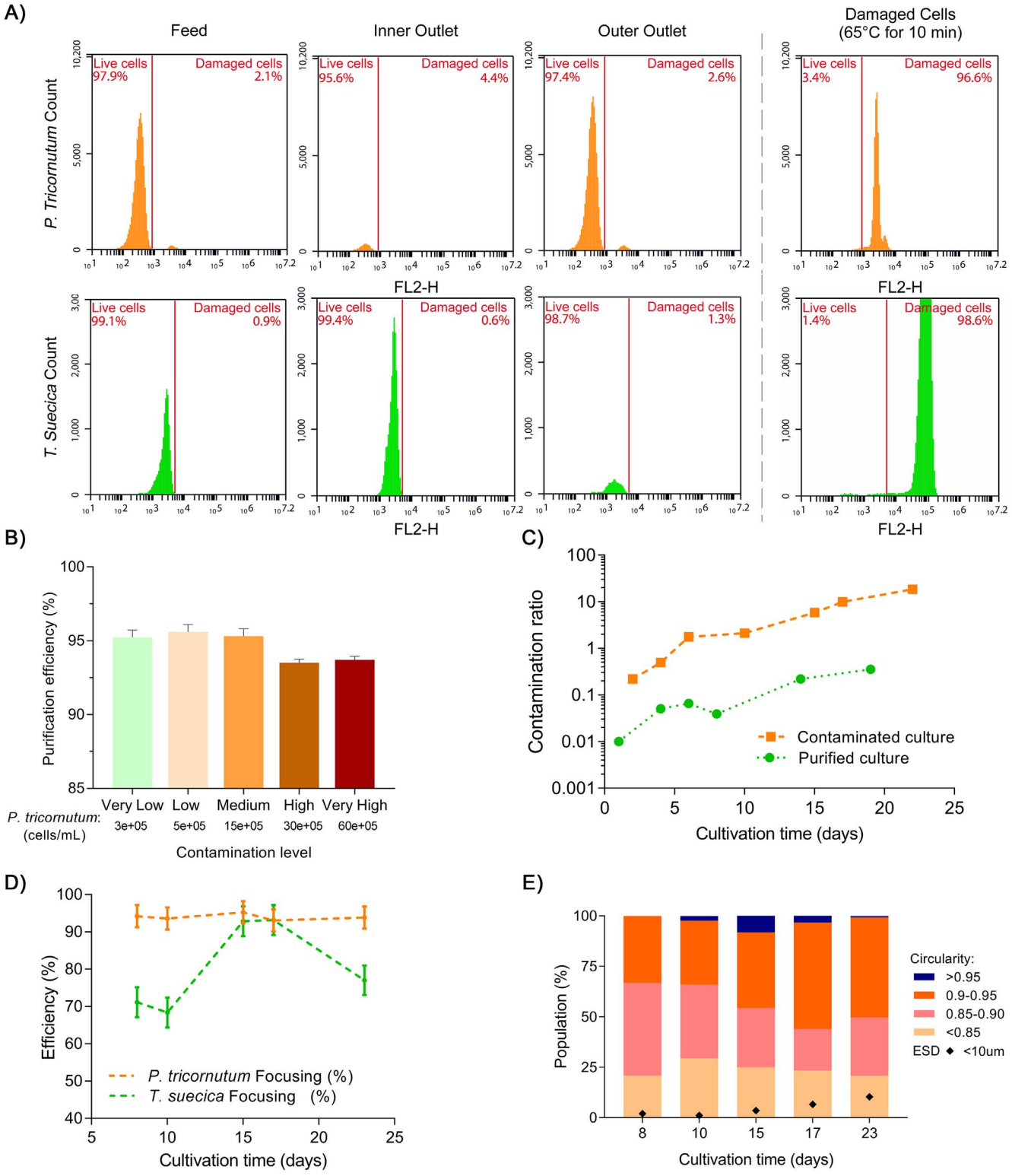

Fig. 5. A) Viability results as obtained using flow cytometer. The red vertical line marks the fluorescence of the PI stain. The cells that cross the line would be indicated to be damaged or lysed as they get stained by PI. The plots on the right represent the lysed cells by keeping them in water bath at 65 °C. The %age of cells that absorb the stain (cross the line) are mentioned as damaged cells in red. B) Purification efficiency as a function of initial contamination level (i.e., concentration of *P. tricornutum*), keeping *T. suecica* concentration constant. C) Comparison of the variation in the contamination ratio (ratio of *P. tricornutum* to *T. suecica* cell concentrations) for purified inoculum and contaminated culture over ~3 weeks. Note that in purified inoculum culture, the *P. tricornutum* concentration remained ~50 times lower, D) Selective separation tests performed on different days of cultivation of mixed culture of *P. tricornutum* and *T. suecica.* The highest *T. suecica* focusing was found during the stationary culture phase (days 13–20). E) Bar chart showing the percent of population for different circularity ranges. Dot plot shows the *T. suecica* having effective spherical diameter (ESD) lesser than 10 μm. (For interpretation of the references to colour in this figure legend, the reader is referred to the web version of this article.)

these cells was always more than 90%. Thus, it can be concluded that the purification efficiency obtained by this present methodology is relative insensitive to variation of *P. tricornutum* cell concentrations between 0.3 million cells/mLand 6 million cells/mL.

3.3.3. Contamination ratio over time after purification

A purified sample of *T. suecica* obtained from the inner outlet at 1 mL/min was re-inoculated in the marine medium and the cell concentration was monitored over time to assess the contamination ratio over time after purification (Fig. 5C). It seemed that invasion of *P. tricornutum* remained suppressed until day 10. After this time, the concentration of *P. tricornutum* increased but very gradually such that by the end of third week of cultivation, the contamination ratio (ratio of concentrations of *P. tricornutum* to *T. suecica*) was 50 times lower for the purified culture as compared to invaded one (Fig. 5C). However, it was observed in a separate experiment that inoculating this purified culture at day 14 in a fresh medium resulted in negligible re-contamination of *P. tricornutum* since its concentration was still too low to grow. However, if re-contamination does occur, multiple cycles of separation can be applied at 13–20 days intervals to maintain the desired level of purification.

3.3.4. Purification as function of cultivation time

As a final set of experiments, several purification tests were conducted as function of cultivation time in a mixed culture of *P. tricornutum* and *T. suecica* to verify the effect of relative cell concentration of both species over time (Fig. 5D). This series of experiments started from the 8th day of the culture when there were sufficient cell populations of both strains until the third week of the culture when the cells of *T. suecica* entered declining growth phase. No significant variation in purification efficiency was observed over time. However, there were noteworthy changes in the focusing efficiency of *T. suecica* from the early second week until day 23.

In the second week of the culture, the microalgal cells were in their exponential growth phase, having a large number of dividing cells and those that had higher ESD and were more elliptical. At the end of the second week, the cells enter their stationary phase in which the cell division rate decreased and the cells became more uniform in size and more circular. Microalgae cell physiology and morphology change as function of cultivation stage, which can affect the performance of sensitive microfluidic devices, a factor which has been reported for *Euglena* sp. (Li et al., 2017). On day 15 and 17, roughly 50% of the *T. suecica* population had a circularity of greater than 0.9 (Fig. 5E), which tended to focus better inside the channel (Fig. 5D). However, by the end of 3rd week, the *T. suecica* cells began to deteriorate due to nutrition competition as the concentration of *P. tricornutum* cells increased to 6 million cells/mL. This apparently influenced the morphology of the *T. suecica* cells again. Consequently on day 23, there was an increase in the population of cells smaller than the effective spherical diameter of 10 μm, along with a reduced circularity which accounted for decline in *T. suecica* focusing efficiency. Thus, the changes in focusing efficiency were related to the significant variation in cell size as well as cell shape of the *T. suecica* cells in the second-third week.

These results show that due to high sensitivity of the device to cell size and shape, there is an optimum cultivation time for separation. In terms of the feasibility of trapezoidal microchannels for algal separation, we can conclude that the device demonstrated the following: (a) near 100% viability of both separated species, (b) independence of separation on concentration, and (c) suppression of contamination after re-cultivation of the purified sample. From these results the potential of this technology as a feasible microalgal contamination mitigation technique has been validated. Future research should focus on high-throughput multiplexed systems (Rafeie et al., 2016; Warkiani et al., 2015) and on selective segregation of more than two species in complex microalgae consortia.

4. Conclusion

This study demonstrates the performance and feasibility of a spiral microchannel for selective separation and purification of *Tetraselmis suecica* cultures contaminated with an invasive diatom, *Phaeodactylum tricornutum*. At the optimum flow rate, up to 95% of the *P. tricornutum* cells were separated from the culture, while also capturing up to 90% of *T. suecica* cells. Using this technique the cells were fractionated without any noticeable loss in viability of either species. Overall, this study should open up a new, low-cost method for selective microalgae separation at both laboratory scales (now) and potentially at commercial scales (in future) with parallelization.

Acknowledgements

D. Vandamme is a postdoctoral Researcher funded by the Research Foundation – Flanders Belgium (FWO – 12D8917N). R. Taylor would like to acknowledge the fellowship support of the Australian Research Council (ARC – DE160100131). M.E.W. would like to acknowledge the support of the Australian Research Council through a Discovery Project Grant (DP170103704).

Appendix A. Supplementary data

Supplementary data associated with this article can be found, in the online version, at http://dx.doi.org/10.1016/j.biortech.2017.12.065.

References

Asmolov, E.S., 1999. The inertial lift on a spherical particle in a plane Poiseuille flow at large channel Reynolds number. J. Fluid Mech. 381, 63–87.
Augustsson, P., Magnusson, C., Nordin, M., Lilja, H., Laurell, T., 2012. Microfluidic, label-free enrichment of prostate cancer cells in blood based on acoustophoresis. Anal. Chem. 84 (18), 7954–7962.
Bartley, M.L., Boeing, W.J., Corcoran, A.A., Holguin, F.O., Schaub, T., 2013. Effects of salinity on growth and lipid accumulation of biofuel microalga Nannochloropsis salina and invading organisms. Biomass Bioenergy 54, 83–88.
Berger, S., Talbot, L., Yao, L., 1983. Flow in curved pipes. Annu. Rev. Fluid Mech. 15 (1), 461–512.
Bhagat, A.A.S., Kuntaegowdanahalli, S.S., Kaval, N., Seliskar, C.J., Papautsky, I., 2010. Inertial microfluidics for sheath-less high-throughput flow cytometry. Biomed. Microdevices 12 (2), 187–195.
Brennan, L., Owende, P., 2010. Biofuels from microalgae—A review of technologies for production, processing, and extractions of biofuels and co-products. Renew. Sustain. Energy Rev. 14 (2), 557–577.
Cellamare, M., Rolland, A., Jacquet, S., 2010. Flow cytometry sorting of freshwater phytoplankton. J. Appl. Phycol. 22 (1), 87–100.
Chisti, Y., 2007. Biodiesel from microalgae. Biotechnol. Adv. 25 (3), 294–306.
Di Carlo, D., 2009. Inertial microfluidics. Lab Chip 9 (21), 3038–3046.
Di Carlo, D., Edd, J.F., Humphry, K.J., Stone, H.A., Toner, M., 2009. Particle segregation and dynamics in confined flows. Phys. Rev. Lett. 102 (9), 094503.
Di Carlo, D., Irimia, D., Tompkins, R.G., Toner, M., 2007. Continuous inertial focusing, ordering, and separation of particles in microchannels. Proc. Natl. Acad. Sci. U.S.A. 104 (48), 18892–18897.
Ghim, C.-M., Kim, T., Mitchell, R.J., Lee, S.K., 2010. Synthetic biology for biofuels: building designer microbes from the scratch. Biotechnol. Bioprocess Eng. 15 (1), 11–21.
Goldman, J.C., Azov, Y., Riley, C.B., Dennett, M.R., 1982. The effect of pH in intensive microalgal cultures. I. Biomass regulation. J. Exp. Mar. Biol. Ecol. 57 (1), 1–13.
Goldman, J.C., Stanley, H.I., 1974. Relative growth of different species of marine algae in wasterwater-seawater mixtures. Mar. Biol. 28 (1), 17–25.
Guan, G., Wu, L., Bhagat, A.A., Li, Z., Chen, P.C.Y., Chao, S., Ong, C.J., Han, J., 2013. Spiral microchannel with rectangular and trapezoidal cross-sections for size based particle separation. Sci. Rep. 3, 1475.
Han, A., Hou, H., Li, L., Kim, H.S., de Figueiredo, P., 2013. Microfabricated devices in microbial bioenergy sciences. Trends Biotechnol. 31 (4), 225–232.
Hashemi, N., Erickson, J.S., Golden, J.P., Jackson, K.M., Ligler, F.S., 2011. Microflow Cytometer for optical analysis of phytoplankton. Biosens. Bioelectron. 26 (11), 4263–4269.
Heyt, J., Diaz, J., 1975. Pressure drop in flat-oval spiral air duct. ASHRAE Trans. 81 (Part 2), 221–230.
Hønsvall, B.K., Altin, D., Robertson, L.J., 2016. Continuous harvesting of microalgae by new microfluidic technology for particle separation. Bioresour. Technol. 200, 360–365.
Hood, K., Lee, S., Roper, M., 2015. Inertial migration of a rigid sphere in three-dimensional Poiseuille flow. J. Fluid Mech. 765, 452–479.
Hoshaw, R., Rosowski, J., 1973. Methods for microscopic algae. In: Handbook of

Phycological Methods. Cambridge University Press, New York, pp. 53–67.
Huang, Y.-T., Su, C.-P., 2014. High lipid content and productivity of microalgae cultivating under elevated carbon dioxide. Int. J. Environ. Sci. Technol. 11 (3), 703–710.
Hyka, P., Lickova, S., Přibyl, P., Melzoch, K., Kovar, K., 2013. Flow cytometry for the development of biotechnological processes with microalgae. Biotechnol. Adv. 31 (1), 2–16.
Iliescu, C., Xu, G., Barbarini, E., Avram, M., Avram, A., 2008. Microfluidic device for continuous magnetophoretic separation of white blood cells. Microsyst. Technol. 15 (8), 1157–1162.
Jokerst, J.C., Emory, J.M., Henry, C.S., 2012. Advances in microfluidics for environmental analysis. Analyst 137 (1), 24–34.
Juang, Y.-J., Chang, J.-S., 2016. Applications of microfluidics in microalgae biotechnology: a review. Biotechnol. J. 11 (3), 327–335.
Kemna, E.W., Schoeman, R.M., Wolbers, F., Vermes, I., Weitz, D.A., van den Berg, A., 2012. High-yield cell ordering and deterministic cell-in-droplet encapsulation using Dean flow in a curved microchannel. Lab Chip 12 (16), 2881–2887.
Koch, R., 2010. Zur untersuchung von pathogenen organismen.
Kuntaegowdanahalli, S.S., Bhagat, A.A., Kumar, G., Papautsky, I., 2009. Inertial microfluidics for continuous particle separation in spiral microchannels. Lab Chip 9 (20), 2973–2980.
Lama, S., Muylaert, K., Karki, T.B., Foubert, I., Henderson, R.K., Vandamme, D., 2016. Flocculation properties of several microalgae and a cyanobacterium species during ferric chloride, chitosan and alkaline flocculation. Bioresour. Technol. 220, 464–470.
Li, M., Muñoz, H., Schmidt, A., Guo, B., Lei, C., Goda, K., Di Carlo, D., 2016. Inertial focusing of ellipsoidal Euglena gracilis cells in a stepped microchannel. Lab Chip 16 (22), 4458–4465.
Li, M., Muñoz, H.E., Goda, K., Di Carlo, D., 2017. Shape-based separation of microalga Euglena gracilis using inertial microfluidics. Sci. Rep. 7 (1), 10802.
Li, W., Gao, K., Beardall, J., 2012. Interactive effects of ocean acidification and nitrogen-limitation on the diatom *Phaeodactylum tricornutum*. PLoS One 7 (12), e51590.
Paik, S.-M., Sim, S.-J., Jeon, N.L., 2017. Microfluidic perfusion bioreactor for optimization of microalgal lipid productivity. Bioresour. Technol. 233 (Supplement C), 433–437.
Rafeie, M., Zhang, J., Asadnia, M., Li, W., Warkiani, M.E., 2016. Multiplexing slanted spiral microchannels for ultra-fast blood plasma separation. Lab Chip 16 (15), 2791–2802.
Rodolfi, L., Chini Zittelli, G., Bassi, N., Padovani, G., Biondi, N., Bonini, G., Tredici, M.R., 2009. Microalgae for oil: strain selection, induction of lipid synthesis and outdoor mass cultivation in a low-cost photobioreactor. Biotechnol. Bioeng. 102 (1), 100–112.
Ruiz, J., Olivieri, G., de Vree, J., Bosma, R., Willems, P., Reith, J.H., Eppink, M.H.M., Kleinegris, D.M.M., Wijffels, R.H., Barbosa, M.J., 2016. Towards industrial products from microalgae. Energy Environ. Sci. 9 (10), 3036–3043.
Schaap, A., Dumon, J., Den Toonder, J., 2016. Sorting algal cells by morphology in spiral microchannels using inertial microfluidics. Microfluid. Nanofluid. 20 (9), 125.
Segre, G., 1961. Radial particle displacements in Poiseuille flow of suspensions. Nature 189, 209–210.
Sei, Y., Justus, K., LeDuc, P., Kim, Y., 2014. Engineering living systems on chips: from cells to human on chips. Microfluid. Nanofluid. 16 (5), 907–920.
Sensen, C.W., Heimann, K., Melkonian, M., 1993. The production of clonal and axenic cultures of microalgae using fluorescence-activated cell sorting. Eur. J. Phycol. 28 (2), 93–97.
Shakeel Syed, M., Rafeie, M., Henderson, R., Vandamme, D., Asadnia, M., Ebrahimi Warkiani, M., 2017. A 3D-printed mini-hydrocyclone for high throughput particle separation: application to primary harvesting of microalgae. Lab Chip 17 (14), 2459–2469.
Sinigalliano, C.D., Winshell, J., Guerrero, M.A., Scorzetti, G., Fell, J.W., Eaton, R.W., Brand, L., Rein, K.S., 2009. Viable cell sorting of dinoflagellates by multiparametric flow cytometry. Phycologia 48 (4), 249–257.
Skommer, J., Wlodkowic, D., 2015. Successes and future outlook for microfluidics-based cardiovascular drug discovery. Expert Opin. Drug Discov. 10 (3), 231–244.
Wan, C., Alam, M.A., Zhao, X.-Q., Zhang, X.-Y., Guo, S.-L., Ho, S.-H., Chang, J.-S., Bai, F.-W., 2015. Current progress and future prospect of microalgal biomass harvest using various flocculation technologies. Bioresour. Technol. 184, 251–257.
Warkiani, M.E., Tay, A.K., Guan, G., Han, J., 2015. Membrane-less microfiltration using inertial microfluidics. Sci. Rep. 5, 11018.
Wu, C., Lillehoj, P.B., Sabet, L., Wang, P., Ho, C.M., 2011. Ultrasonication on a microfluidic chip to lyse single and multiple Pseudo-nitzschia for marine biotoxin analysis. Biotechnol. J. 6 (2), 150–155.
Wu, L., Guan, G., Hou, H.W., Bhagat, A.A.S., Han, J., 2012. Separation of leukocytes from blood using spiral channel with trapezoid cross-section. Anal. Chem. 84 (21), 9324–9331.
Yetisen, A.K., Akram, M.S., Lowe, C.R., 2013. Paper-based microfluidic point-of-care diagnostic devices. Lab Chip 13 (12), 2210–2251.
Zhou, J., Papautsky, I., 2013. Fundamentals of inertial focusing in microchannels. Lab Chip 13 (6), 1121–1132.